Phylogenetic ctDNA analysis depicts early stage lung cancer evolution

Christopher Abbosh[1*], Nicolai J. Birkbak[1,2*], Gareth A. Wilson[1,2*], Mariam Jamal-Hanjani[1*], Tudor Constantin[3*], Raheleh Salari[3*], John Le Quesne[4*], David A Moore[4+], Selvaraju Veeriah[1+], Rachel Rosenthal[1+], Teresa Marafioti[1,5], Eser Kirkizlar[3], Thomas B K Watkins[1,2], Nicholas McGranahan[1,2], Sophia Ward[1,2,6], Luke Martinson[4], Joan Riley[4], Francesco Fraioli[7], Maise Al Bakir[2], Eva Gronroos[2], Francisco Zambrana[1], Raymondo Endozo[7], Wenya Linda Bi[8,9], Fiona M. Fennessy[8,9], Nicole Sponer[3], Diana Johnson[1], Joanne Laycock[1], Seema Shafi[1], Justyna Czyzewska-Khan[1], Andrew Rowan[2], Tim Chambers[2,6], Nik Matthews[6,10], Samra Turajlic[2,11], Crispin Hiley1[2], Siow Ming Lee[12,1], Martin Forster[1,12], Tanya Ahmad[12], Mary Falzon[5], Elaine Borg[5], David Lawrence[13], Martin Hayward[13], Shyam Kolvekar[13], Nikolaos Panagiotopoulos[13], Sam M Janes[1,14,15], Ricky Thakrar[14], Asia Ahmed[16], Fiona Blackhall[17,18], Yvonne Summers[18], Dina Hafez[3], Ashwini Naik[3], Apratim Ganguly[3], Stephanie Kareht[3], Rajesh Shah[19], Leena Joseph[20], Anne Marie Quinn[20], Phil Crosbie[21], Babu Naidu[22], Gary Middleton[23], Gerald Langman[24], Simon Trotter[24], Marianne Nicolson[25], Hardy Remmen[26], Keith Kerr[27], Mahendran Chetty[28], Lesley Gomersall[29], Dean Fennell[4], Apostolos Nakas[30], Sridhar Rathinam[30], Girija Anand[31], Sajid Khan[32,33], Peter Russell[34], Veni Ezhil[35], Babikir Ismail[36], Melanie Irvin-sellers[37], Vineet Prakash[38], Jason Lester[39], Malgorzata Kornaszewska[40], Richard Attanoos[41], Haydn Adams[42], Helen Davies[43], Dahmane Oukrif[1], Ayse U Akarca[1], John A Hartley[44], Helen L Lowe[44], Sara Lock[45], Natasha Iles[46], Harriet Bell[46], Yenting Ngai[46], Greg Elgar[2,6], Zoltan Szallasi[47,48,49], Roland F Schwarz[50], Javier Herrero[51], Aengus Stewart[52], Sergio A Quezada[53], Peter Van Loo[54,55], Caroline Dive[56], Jimmy Lin[3], Matthew Rabinowitz[3], Hugo JWL Aerts[8,9,57], Allan Hackshaw[45], Jacqui A Shaw[4], Bernhard G. Zimmermann[3], and Charles Swanton[1,2] on behalf of the TRACERx and PEACE consortia.

*These authors contributed equally to this work +These authors contributed equally to this work

1. Cancer Research UK Lung Cancer Centre of Excellence, University College London Cancer Institute, Paul O'Gorman Building, 72 Huntley Street, London, WC1E 6BT
2. Translational Cancer Therapeutics Laboratory, The Francis Crick Institute, 1 Midland Rd, London NW1 1AT
3. Natera Inc., 201 Industrial Rd., San Carlos, United States, CA 94070
4. Cancer Studies, University of Leicester, Leicester, United Kingdom, LE2 7LX
5. Department of Pathology, University College London Hospitals, 235 Euston Rd, Fitzrovia, London, United Kingdom, NW1 2BU
6. Advanced Sequencing Facility, The Francis Crick Institute, 1 Midland Rd, London NW1 1AT
7. Department of Nuclear Medicine, University College London Hospitals, 235 Euston Rd, Fitzrovia, London, United Kingdom, NW1 2BU
8. Brigham and Women's Hospital, Boston, MA 02115, USA
9. Harvard Medical School, Boston, MA 02115, USA
10. Tumour Profiling Unit Genomics Facility, The Institute of Cancer Research, 237 Fulham Road, London, SW3 6JB
11. Renal and Skin Units, The Royal Marsden Hospital, London, SW3 6JJ
12. Department of Oncology, University College London Hospitals, 235 Euston Rd, Fitzrovia, London, United Kingdom, NW1 2BU
13. Department of Cardiothoracic Surgery, University College London Hospitals, 235 Euston Rd, Fitzrovia, London, United Kingdom, NW1 2BU
14. Department of Respiratory Medicine, University College London Hospitals, 235 Euston Rd, Fitzrovia, London, United Kingdom, NW1 2BU
15. Lungs for Living Research Centre. Division of Medicine, Rayne Building. University College London, 5 University Street. London. WC1E 6JF

16. Department of Radiology, University College London Hospitals, 235 Euston Rd, Fitzrovia, London, United Kingdom, NW1 2BU
17. Institute of Cancer Studies, University of Manchester, Oxford Road, Manchester, M13 9PL
18. The Christie Hospital, Manchester, United Kingdom, M20 4BX
19. Department of Cardiothoracic Surgery, University Hospitals of South Manchester, Manchester, M23 9LT
20. Department of Pathology, University Hospitals of South Manchester, Manchester, M23 9LT
21. North West Lung Centre, University Hospital of South Manchester, Manchester, United Kingdom, M23 9LT
22. Department of Thoracic Surgery, Birmingham Heartlands Hospital, Birmingham, United Kingdom, B9 5SS
23. Department of Medical Oncology, Birmingham Heartlands Hospital, Birmingham, United Kingdom, B9 5SS
24. Department of Cellular Pathology, Birmingham Heartlands Hospital, Birmingham, United Kingdom, B9 5SS
25. Department of Medical Oncology, Aberdeen University Medical School & Aberdeen Royal Infirmary, Aberdeen, Scotland, United Kingdom, AB25 2ZN
26. Department of Cardiothoracic Surgery, Aberdeen University Medical School & Aberdeen Royal Infirmary, Aberdeen, United Kingdom, AB25 2ZD
27. Department of Pathology, Aberdeen University Medical School & Aberdeen Royal Infirmary, Aberdeen, Scotland, United Kingdom, AB25 2ZD
28. Department of Respiratory Medicine, Aberdeen University Medical School & Aberdeen Royal Infirmary, Aberdeen, United Kingdom, AB25 2ZN

29. Department of Radiology, Aberdeen University Medical School & Aberdeen Royal Infirmary, Aberdeen, Scotland, United Kingdom, AB25 2ZN
30. Department of Thoracic Surgery, Glenfield Hospital, Leicester, LE3 9QP
31. Department of Radiotherapy, North Middlesex University Hospital, London N18 1QX
32. Department of Respiratory Medicine, Royal Free Hospital, Pond Street, London, NW3 2QG
33. Department of Respiratory Medicine, Barnet and Chase Farm Hospitals, Wellhouse Lane, Barnet, United Kingdom, EN5 3DJ
34. Department of Respiratory Medicine, The Princess Alexandra Hospital, Hamstel Rd, Harlow CM20 1QX
35. Department of Clinical Oncology, St.Luke's Cancer Centre, Royal Surrey County Hospital, Guildford, GU2 7XX
36. Department of Pathology, Ashford and St. Peters' Hospital, Guildford Road, Chertsey, Surrey, KT16 0PZ
37. Department of Respiratory Medicine, Ashford and St. Peters' Hospital, Guildford Road, Chertsey, Surrey, KT16 0PZ
38. Department of Radiology, Ashford and St. Peters' Hospital, Guildford Road, Chertsey, Surrey, KT16 0PZ
39. Department of Clinical Oncology, Velindre Hospital, Cardiff, Wales, United Kingdom, CF14 2TL
40. Department of Cardiothoracic Surgery, University Hospital Llandough, Cardiff, Wales, United Kingdom, CF64 2XX
41. Department of Pathology, University Hospital Llandough, Cardiff, Wales, United Kingdom, CF64 2XX

42. Department of Radiology, University Hospital Llandough, Cardiff, Wales, United Kingdom, CF64 2XX
43. Department of Respiratory Medicine, University Hospital Llandough, Cardiff, Wales, United Kingdom, CF64 2XX
44. UCL ECMC GCLP Facility, University College London Cancer Institute, Paul O'Gorman Building, 72 Huntley Street, London, WC1E 6BT
45. Department of Respiratory Medicine, The Whittington Hospital NHS Trust, United Kingdom, N19 5NF
46. University College London, Cancer Research UK & UCL Cancer Trials Centre, London, United Kingdom, W1T 4TJ
47. Centre for Biological Sequence Analysis, Department of Systems Biology, Technical University of Denmark, 2800 Lyngby, Denmark.
48. Computational Health Informatics Program (CHIP), Boston Children's Hospital, Harvard Medical School, Boston, MA, USA.
49. MTA-SE-NAP, Brain Metastasis Research Group, 2nd Department of Pathology, Semmelweis University, 1091 Budapest, Hungary.
50. Berlin Institute for Medical Systems Biology, Max Delbrueck Center for Molecular Medicine, Berlin, Germany
51. Bill Lyons Informatics Centre, University College London Cancer Institute, Paul O'Gorman Building, 72 Huntley Street, London, WC1E 6BT
52. Department of Bioinformatics and Biostatistics, The Francis Crick Institute, 1 Midland Rd, London NW1 1AT
53. Cancer Immunology Unit, University College London Cancer Institute, Paul O'Gorman Building, 72 Huntley Street, London, WC1E 6BT

54. Cancer Genomics Laboratory, The Francis Crick Institute, 1 Midland Rd, London NW1 1AT
55. Department of Human Genetics, University of Leuven, B-3000 Leuven, Belgium
56. Cancer Research UK Manchester Institute, Manchester, United Kingdom, M20 4BX
57. Dana-Farber Cancer Institute, 450 Brookline Ave. Boston, United States, MA 02215-5450

Corresponding author:

Charles Swanton

Translational Cancer Therapeutics Laboratory

The Francis Crick Institute

3rd Floor South West

1 Midland Road

London

NW1 1A

Email: Charles.Swanton@crick.ac.uk

Office +44 203 796 2047

Summary (156 words)

Earlier detection of relapse following primary surgery for non-small cell lung cancer and the characterization of emerging subclones seeding metastatic sites might offer new therapeutic approaches to limit tumor recurrence. The potential to non-invasively track tumor evolutionary dynamics in ctDNA of early-stage lung cancer is not established. Here we conduct a patient-specific approach to ctDNA profiling in the first 100 lung TRACERx (**TRA**cking **C**ancer **E**volution through therapy (**Rx**)) study participants, including one patient co-recruited to the PEACE (**P**osthumous **E**valuation of **A**dvanced **C**ancer **E**nvironment) post-mortem study. We identify independent predictors of ctDNA release in early-stage non-small cell lung cancer and perform tumor volume limit of detection analyses. Through blinded profiling of post-operative plasma, we observe evidence of adjuvant chemotherapy resistance and identify patients destined to experience recurrence of their lung cancer. Finally, we show that phylogenetic ctDNA profiling tracks the subclonal nature of lung cancer relapse and metastases, providing a new approach for ctDNA driven therapeutic studies

Main text

Lung cancer is the leading cause of cancer death worldwide[1-2]. Established metastatic non-small cell lung cancer (NSCLC) cannot be cured with systemic chemotherapy. Yet clinical studies have shown a 5% benefit of post-operative (adjuvant) chemotherapy on overall survival[3]. This modest survival benefit may reflect a vulnerability of treating low volume disease within the context of reduced intra-tumor heterogeneity[4]. Improving adjuvant treatment of lung cancer could improve cure rates. However, achieving this objective will require the development of a diagnostic platform capable of identifying, monitoring and genomically characterizing recurring or residual disease early. This would create a therapeutic setting where only patients destined to recur would receive treatment, where intervention could be directed to the evolving tumor subclone seeding metastatic recurrence guided by clinical trials powered to determine treatment effect within smaller patient cohorts.

Circulating tumor DNA (ctDNA) detection in plasma has been shown in breast[5,6] and colorectal cancer[7] to detect minimal residual disease in the adjuvant setting and identify patients destined to relapse post-operatively in advance of established clinical parameters. Here, we report a bespoke multiplex-PCR NGS approach to ctDNA profiling within the context of the

prospective tumor evolutionary NSCLC study TRACERx. We address determinants of ctDNA detection in early-stage NSCLC and investigate the ability of ctDNA to identify and genomically characterize, at subclone resolution, post-operative NSCLC relapse using a tumor phylogenetic framework.

Phylogenetic ctDNA profiling

The TRACERx study monitors the clonal evolution of NSCLC from diagnosis through to relapse and death[8]. Using multi-region exome sequencing (M-Seq) derived tumor phylogenetic trees developed through prospective analysis of the 100 patient TRACERx cohort, we conducted a phylogenetic approach to ctDNA profiling in early stage NSCLC **(Fig. 1).** Bespoke multiplex-PCR assay-panels were synthesised for each patient, targeting clonal and subclonal single nucleotide variants (SNVs) selected to track phylogenetic tumor branches in plasma **(Fig 1.)**. Analytical validation of the multiplex-PCR NGS platform demonstrated a sensitivity of above 99% for the detection of SNVs at frequencies above 0.1% and the specificity of detecting a single SNV was 99.6% (**Extended Data Fig 1a**). At least two SNVs were detected in ctDNA from each NSCLC analyzed in our published discovery cohort data[9], demonstrating biological sensitivity of a two SNV threshold for ctDNA detection in early-stage NSCLC. Therefore, we

prospectively selected a threshold of two detected SNVs for calling a sample ctDNA positive for validation within this study - to minimize type I error in a platform testing up to 30 tumour-specific SNVs per time-point in a single patient (see **Extended Data Fig 1b** for justification**)**. Cross-platform validation was performed in 28 patients with M-Seq confirmed SNV(s) within one or more hotspots targeted by a generic multiplex PCR-NGS panel **(Extended Table 1a-b, Supplementary Table 1).** All 18 bespoke-panel ctDNA negative patients had no tumor SNVs detectable in plasma pre-operatively by the generic panel supporting biological specificity of the targeted approach, 7 of 10 bespoke-panel ctDNA positive patients had tumor SNVs detected in plasma by the generic panel **(Extended Table 1a-b).**

Determinants of ctDNA detection in NSCLC

We sought to identify clinicopathological determinants of ctDNA detection in early-stage NSCLC by profiling pre-operative plasma samples in 96 of 100 TRACERx patients (cohort, sample characteristics **Extended Table 2a-c, Supplementary Table 2**). It was not possible to analyze samples from four patients (see **Extended Data Fig 2a** for details**)**. Individual patient assay-panels were designed to target a median of 18 SNVs (range 10 to 22) comprising a

204 median of 11 clonal SNVs (range 2 to 20) and a median of 6 subclonal SNVs (range 0 to 16)
205 **(Extended Data Fig 2b)**.

206 At least two SNVs were detected in ctDNA pre-operatively in 46 of 96 (48%) early-stage
207 NSCLCs, a single SNV was detected in 12 additional cases **(Fig 2a)**. Centrally reviewed
208 pathological data revealed that ctDNA detection was associated with histological subtype: 97%
209 (30/31) of lung squamous cell carcinomas (LUSCs) and 71% (5 of 7) of other NSCLC subtypes
210 were ctDNA positive, compared with 19% (11/58) of lung adenocarcinomas (LUADs) (**Fig**
211 **2a).** ctDNA detection stratified by TNM stage revealed that 94% (16 of 17) of stage I LUSCs
212 were detected compared with 13% (5 of 39) of stage I LUADs (**Extended Data Fig 3a)**.
213 Passive release of ctDNA into the circulation may be associated with apoptosis and necrosis[10].
214 As expected[11], LUSCs were significantly more necrotic than LUADs and ctDNA positive
215 LUADs formed a sub-group of more necrotic tumors compared with ctDNA negative LUADs
216 **(Extended Data Fig 3b)**. Necrosis, lymph node involvement, lymphovascular invasion,
217 pathological tumor size, Ki67 labelling indices, non-adenocarcinoma histology and total cell-
218 free DNA input predicted ctDNA detection in univariable analyses (**Extended Data Fig 3c**).
219 Multivariable analysis revealed non-adenocarcinoma histology, the presence of lympho-
220 vascular invasion and high Ki67 proliferation index as independent predictors of ctDNA

detection (**Extended Data Fig 3c**). Since FDG-avidity on positron emission tomography (PET) scans correlates with proliferative indices in early-stage NSCLC[12,13], we investigated tumor PET FDG-avidity and ctDNA detection. PET FDG-avidity predicted ctDNA detection (area under curve = 0.84, P<0.001, n=92) (**Extended Data Fig 3d)**. Within LUADs, common driver events in *KRAS, EGFR* or *TP53* were not associated with ctDNA detection (**Extended Data Fig 3e).**

We analyzed the distribution of clonal and subclonal SNVs in ctDNA positive patients. Clonal SNVs were detected in all 46 ctDNA positive patients; a median of 94% (range 11% to 100%) of clonal SNVs targeted by assay-panels were detected in ctDNA. 40 of 46 ctDNA positive patients had subclonal SNVs targeted by assay-panels and subclonal SNVs were detected in 27 (68%) of these patients. A median of 27% (range 0% to 91%) of targeted subclonal SNVs were detected in ctDNA positive patients **(Figure 2b)**. The mean plasma variant allele frequency (VAF) of clonal SNVs was significantly higher than that of subclonal SNVs **(Extended Data Fig 4a)** (within patient comparison, Wilcoxon signed-rank test, P<0.001, n=27, **Supplementary Table 3**) supporting the use of clonal alterations as a more sensitive method of ctDNA detection than subclonal alterations[9,14].

In ctDNA positive patients, macroscopic tumor size correlated with mean clonal plasma VAF (Spearman's Rho = 0.405, P=0.005, n=46) (**Extended Data Fig 4b**). CT scan volumetric analyses were available in 38 of 46 ctDNA positive patients (see **Extended Data Fig 4c**). Tumor volume correlated with mean clonal plasma VAF (**Fig 3a,** Spearman's Rho = 0.61, P<0.001, n=38). A linear relationship between log- transformed volume and mean clonal VAF values was observed (**Fig 3a**). The line of best fit applied to our data was consistent with the line fitted to NSCLC volumetric data and ctDNA plasma VAFs reported in previously published work[15] (**Extended Data Fig 4d)**. Linear modelling based on the TRACERx data approximated that a primary tumor volume of $11cm^3$ would result in a mean clonal plasma VAF of 0.1% **(Figure 3b).** We multiplied tumor purity by tumor volume to control for stromal contamination and determine cancer cell volume (**Extended Data Fig 4e)**. On the assumption that $1cm^3$ of effective tumor contains 9.4×10^7 cells we approximated that a plasma VAF of 0.1% corresponds to a tumor burden of 326 million malignant cells **(Extended Data Fig 4f).**

To investigate predictors of subclone detection we mapped detected subclonal SNVs back to M-seq derived tumor phylogenetic trees. 35 of 57 (61%) shared subclones (identified in more than one tumor region through M-Seq analysis) were identified in ctDNA, compared with 26 of 80 (33%) private subclones (detected in a single tumor region only) **(Extended Data Fig**

4g). This suggested subclone volume influences subclonal ctDNA detection. We estimated subclone volume based on mean regional subclone cancer cell fraction (CCF) and cancer cell volume. Detected subclonal SNVs mapped to subclones with significantly higher estimated volumes than subclones containing undetected SNVs (**Figure 3c)** and subclone volume correlated with subclonal SNV plasma VAF (**Figure 3d**).

Detecting and characterizing NSCLC relapse

The longitudinal phase of the study aimed to determine if ctDNA profiling with patient-specific assay panels could detect and characterize the branched subclone(s) seeding NSCLC relapse. Pre- and post-surgical plasma ctDNA profiling was performed blinded to relapse status in a sub-group of 24 patients (cohort characteristics, **Extended Table 2d-e**). This included relapse free patients who had been followed-up for a median of 775 days (range 688 to 945 days, n=10) and confirmed NSCLC relapse cases (n=14) (cohort design, **Extended Data Fig 2c**). PCR assays were added to panels in this phase of the study to optimize sensitivity in LUADs. A median of 18.5 SNVs (range 12 to 20) were targeted by LUSC assay-panels and a median of 28 SNVs (range 25 to 30) were targeted by LUAD assay-panels (**Extended Data Fig 2d-e).**

Patients were followed up with three to six monthly clinical assessment and chest radiographs. At least 2 SNVs were detected in 13 of 14 (93%) patients with confirmed NSCLC relapse prior to, or at, clinical diagnosis of relapse and detected in 1 of 10 (10%) patients (CRUK0013) with no clinical evidence of NSCLC relapse (**Fig 4a-k, Extended Data Fig 5a-n)**. Excluding a single case where no post-operative plasma was taken prior to clinical relapse (CRUK0041) the median interval between ctDNA detection and NSCLC relapse confirmed on clinically indicated CT imaging (lead-time) was 70 days (range 10 to 346 days). Four of 13 relapse cases exhibited lead-times of more than six months **(Fig 4a-d)**. In two cases ctDNA detection preceded CT imaging inconclusive for NSCLC relapse by 347 days (**Fig 4a**) and 260 days (**Fig 4d**). Post-operative ctDNA profiling reflected adjuvant chemotherapy resistance; CRUK0004, CRUK0080 and CRUK0062 had detectable ctDNA in plasma within 30 days of surgery. The number of detectable SNVs increased in all cases despite adjuvant chemotherapy with disease recurring within 1 year of surgery **(Fig. 4a-c)**. In contrast, CRUK0013 had 20 SNVs detectable in ctDNA 72 hours after surgery and 13 SNVs detectable prior to adjuvant chemotherapy **(Fig 4e).** 51 days following completion of adjuvant treatment, no SNVs were detectable. Two further plasma samples were profiled for this patient at day 457 and 667; ctDNA remained undetectable and the patient remains relapse free 688 days post-surgery **(Fig 4e).** ctDNA

profiling detected intracerebral relapse; CRUK0029 had a pre-operative PET scan performed 50 days prior to surgery demonstrating normal cerebral appearances. Mean clonal plasma VAF of detected SNVs remained above 1% 30 days post-surgery, 54 days post-operatively the patient was confirmed to have intracerebral metastasis **(Fig 4f).**

We sought to resolve subclonal evolutionary-dynamics associated with NSCLC relapse. Subclonal SNVs displaying plasma VAFs similar to clonal SNVs and mapping to phylogenetic clusters confined to a single phylogenetic branch, were detected post-operatively in the ctDNA of four patients who suffered NSCLC relapse (CRUK0004, CRUK0063, CRUK0065 and CRUK0044) **(Fig. 4a,g-i).** These findings suggested a relapse process dominated by a subclone represented in our assay-panel. Notably the subclone implicated by ctDNA as driving the relapse in the case of CRUK0004 contained an ERRB2 (HER2) amplification event that may be targetable in NSCLC[16]**.** This suggests ctDNA defined subclonal evolution may inform precision strategies against emerging subclones **(Fig. 4a).** Relapses involving subclones from more than one phylogenetic branch were evident in patients CRUK0080, CRUK0062 and CRUK0041 **(Fig 4b-c,j).**

Validation of phylogenetic characterization

To validate subclonal ctDNA analyses, data acquired from sequencing metastatic tissue was interpreted with M-seq primary tumor data **(Supplementary Table 4)**. Patient CRUK0063 suffered para-vertebral relapse of their NSCLC. Post-operative ctDNA analysis revealed the detection of the same subclonal SNV (*OR5D18*) on four consecutive occasions over a 231-day period **(Extended Data Fig 6a)**. The *OR5D18* SNV traced back to a subclonal cluster private to primary tumor region three (**Fig 5a)**. Exome sequencing of CT-guided biopsy tissue acquired from the para-vertebral metastasis revealed the subclone implicated in the metastatic event by detection of the *OR5D18* SNV in ctDNA gave rise to the metastatic clone. This supported ctDNA phylogenetic characterization of relapse (**Fig 5a**). The para-vertebral biopsy contained 88 SNVs not present in the primary tumor including an *ARID1A* stop-gain driver SNV. Re-examination of primary tumor region M-Seq data with a lower SNV calling threshold revealed that 16 of 88 SNVs including *ARID1A* were detectable in primary tumor region three, compared to a maximum of 2 of 88 in other tumor regions **(Extended Data Fig 6b).** Since ctDNA implicated the subclone private to primary tumor region three in the relapse process, these data suggest that ctDNA profiling can resolve the primary tumor region from which a low frequency metastatic subclone derives. CRUK0035 developed two liver and one adrenal metastases **(Fig 5b)**. Sequencing of the metastatic liver deposit revealed that only 109 of 149 SNVs classed as

clonal in the primary tumor were detectable in the metastasis. This was suggestive of an ancestral branching event not resolved through primary M-seq analysis **(Figure 5b)**. Post-operative ctDNA profiling identified clonal SNVs present in the liver metastasis biopsy but also revealed SNVs representing a subclone from the primary tumor (**Extended Data Fig 6c)**. This subclone was not present in the metastatic liver deposit **(Fig 5b)**. These data may reflect ctDNA identified from the non-biopsied metastases suggesting multiple metastatic events. CRUK0044 suffered a vertebral and right hilar relapse. Post-operatively the same subclonal SNV (*OR10K1*), was detected in ctDNA on two occasions 85 days apart **(Extended Data Fig 6d)**. This SNV represented a single subclone detected through sequencing hilar lymph-node metastatic tissue, supporting ctDNA findings (**Fig. 5c**). CRUK0041 suffered an intracerebral, hilar and subcarinal lymph node relapse. Four subclonal SNVs representing both branches of the tumor phylogenetic tree were detectable in ctDNA at relapse. Concordant with these data, sequencing of subcarinal metastatic tissue revealed the presence of subclonal SNVs mapping to both phylogenetic branches **(Fig 5d, Extended Data Fig. 6e).** Patient CRUK0013 was found to have lymph-node metastases following primary surgery. Two lymph node metastases were sampled for exome analysis together with M-seq of the primary tumor. Subclonal SNVs detected in ctDNA post-operatively mapped to an ancestral subclone (describing a subclone

that existed during the tumor's evolution) containing a KRAS amplification (**Extended Data Fig 6f, Fig. 5e**). This ancestral subclone was present in the primary tumor and sampled lymph-nodes **(Fig. 5e).** Given the lymph node involvement in this case these findings suggest residual metastatic lymphadenopathy following surgery that responded to adjuvant chemoradiotherapy (**Fig. 4e**)

ctDNA profiling in the metastatic setting

Patient CRUK0063 underwent examination through the PEACE post-mortem study 24 hours following death. Six tumor regions were sampled from three metastatic sites (thoracic vertebral, para-aortic and lung metastases). M-Seq data from the six post-mortem tumor regions (day 857), the para-vertebral relapse biopsy (day 467) and five primary tumor regions (day 0) were combined to infer the phylogenetic structure of this patient's NSCLC (**Fig 6a**). All seven metastatic tumor regions arose from a single ancestral subclone represented by phylogenetic cluster 8 **(Fig 6b).** Six metastatic regions shared a later phylogenetic origin, phylogenetic cluster 12 (**Fig. 6b)**. The single tumor region that had not arisen from phylogenetic cluster 12 was sampled from the para-aortic metastasis at autopsy and contained a private subclone represented by phylogenetic cluster 9 (**Fig 6b).** The findings could represent

two or more independent metastatic events arising from a single branch of the primary tumor phylogenetic tree, with ongoing tumor evolution at each metastatic site **(Fig 6b)**. Or a single metastatic event to the para-aortic site involving the ancestral subclone (phylogenetic cluster 8) prior to evolution of the subclone represented by phylogenetic cluster 9. Followed by metastatic cross-seeding to para-vertebral and lung sites and ongoing clonal evolution (**Fig 6b)**.

We designed a bespoke ctDNA assay-panel to retrospectively track metastatic subclonal burden. 20 clonal SNVs and a median of 8 subclonal SNVs (range 4 to 15) in 9 metastatic subclonal clusters were targeted by the assay-panel **(Extended Data Fig 7).** Since 103 variants per time-point were profiled, SNV call thresholds were increased to maintain platform specificity of more than 99.2% at the 2 SNV ctDNA detection threshold (**see Extended Methods**). ctDNA detection occurred at day 340 post-surgery (**Fig 6c, Extended Data Fig 7**). At day 466 following clinical-relapse at the thoracic para-vertebral site, 18 of 20 SNVs mapping to phylogenetic clusters (8,11 and 12) were detected in ctDNA (**Fig 6c**, **Extended Data Fig 7**). These subclonal clusters were shared between six of seven metastatic sites **(Fig 6b)**. A single SNV from a private subclone (phylogenetic cluster 9) was also detectable in ctDNA at day 466 **(Fig 6c, Extended Data Fig 7)**. This subclone was not identified in the CT guided para-vertebral biopsy taken at day 467 (**Fig 6b)**. The mean plasma VAF of the 18 SNVs

detected in phylogenetic clusters 11, 8 and 12 reflected their proximity to the clonal cluster (light blue) in the M-Seq derived phylogenetic tree **(Fig 6c)**. This suggested a tiered burden of subclonal disease concordant with M-seq phylogenetic inferences **(Fig 6a).** Mean clonal VAF fell in response to palliative radiotherapy and chemotherapy but at day 767 increased **(Fig 6c)**. Single SNVs mapping to phylogenetic clusters 5 and 9 and two SNVs mapping to phylogenetic cluster 2 were now detectable in ctDNA 90 days before death **(Fig 6a-c, Extended Data Fig 7).** These phylogenetic clusters represented subclones private to the para-aortic metastases **(Fig 6a-b)**. Consistent with these data significant para-aortic progression was observed at post-mortem compared with most recent CT imaging performed 112 days before death - which showed no evidence of para-aortic disease.

Discussion

In summary, we find predictors of ctDNA detection in early-stage NSCLC characterized by non-adenocarcinoma histology, necrosis, increased proliferative indices and lymphovascular invasion **(Fig 2a)**. Triple negative breast cancers display necrosis[17], high proliferative indices[18,19] and are associated with increased ctDNA levels compared with other breast cancer subtypes[6] suggesting extension of observations to other tumor types.

We find a relationship between tumor volume and ctDNA detection. We estimate that a primary NSCLC tumor with a volume of $11cm^3$ is required to achieve a ctDNA plasma VAF of 0.1% (**Fig. 3b**), a VAF reflecting the optimum sensitivity of most current ctDNA platforms. Low-dose CT lung screening can identify lung nodules with diameters as low as 4mm[20]. Assuming a spherical nodule, this would translate to a volume of $0.034cm^3$ and an approximate plasma VAF of 1.4×10^{-4} % - at the extreme of detection limits of ctDNA platforms[21]. Sensitivity of ctDNA NSCLC screening may therefore be constrained by tumor size using current technologies. ctDNA release dynamics may alter at disease relapse - in three LUAD cases we detect no ctDNA pre-operatively, yet detect ctDNA at relapse in the absence of clinically detectable disease (**Fig 4a,d,i**).

Targeted ctDNA profiling characterized the subclonal dynamics of relapsing NSCLC. Limitations to this approach include cost, estimated at $1750 per patient for single region tumor sequencing with evaluation of five plasma samples and synthesis of bespoke assay-panels within a clinically relevant timeframe. Adjuvant platinum-based chemotherapy in NSCLC improves cure rates following surgery in only 5% of patients and 20% patients receiving chemotherapy experience acute toxicities[22]. There is an urgent need to increase adjuvant therapy efficacy and better target its use. Our findings indicate that drug development guided

by ctDNA platforms to identify residual disease, define treatment response and target emerging subclones in the adjuvant NSCLC setting, with appropriate CLIA validation, are now feasible.

References

1. Jemal A, Bray F, Center MM, Ferlay J, Ward E, Forman D. Global cancer statistics. CA: A Cancer Journal for Clinicians 2011;61(2):69-90.
2. Siegel RL, Miller KD, Jemal A. Cancer statistics, 2017. CA: A Cancer Journal for Clinicians 2017;67(1):7-30.
3. Pignon J-P, Tribodet H, Scagliotti GV, Douillard J-Y, Shepherd FA, Stephens RJ, et al. Lung Adjuvant Cisplatin Evaluation: A Pooled Analysis by the LACE Collaborative Group. Journal of Clinical Oncology 2008;26(21):3552-9.
4. Landau Dan A, Carter Scott L, Stojanov P, McKenna A, Stevenson K, Lawrence Michael S, et al. Evolution and Impact of Subclonal Mutations in Chronic Lymphocytic Leukemia. Cell;152(4):714-26.
5. Beaver JA, Jelovac D, Balukrishna S, Cochran RL, Croessmann S, Zabransky DJ, et al. Detection of Cancer DNA in Plasma of Patients with Early-Stage Breast Cancer. Clinical Cancer Research 2014;20(10):2643-50.
6. Garcia-Murillas I, Schiavon G, Weigelt B, Ng C, Hrebien S, Cutts RJ, et al. Mutation tracking in circulating tumor DNA predicts relapse in early breast cancer. Science Translational Medicine 2015;7(302):302ra133-302ra133.
7. Tie J, Wang Y, Tomasetti C, Li L, Springer S, Kinde I, et al. Circulating tumor DNA analysis detects minimal residual disease and predicts recurrence in patients with stage II colon cancer. Science Translational Medicine 2016;8(346):346ra92-ra92.
8. Jamal-Hanjani M, Hackshaw A, Ngai Y, Shaw J, Dive C, Quezada S, et al. Tracking genomic cancer evolution for precision medicine: the lung TRACERx study. PLoS Biol 2014;12(7):e1001906.
9. Jamal-Hanjani M, Wilson GA, Horswell S, Mitter R, Sakarya O, Constantin T, et al. Detection of ubiquitous and heterogeneous mutations in cell-free DNA from patients with early-stage non-small-cell lung cancer. Annals of Oncology 2016;27(5):862-7.
10. Jr LAD, Bardelli A. Liquid Biopsies: Genotyping Circulating Tumor DNA. Journal of Clinical Oncology 2014;32(6):579-86.
11. Caruso R, Parisi A, Bonanno A, Paparo D, Quattrocchi E, Branca G, et al. Histologic coagulative tumour necrosis as a prognostic indicator of aggressiveness in renal, lung, thyroid and colorectal carcinomas: A brief review. Oncology Letters 2012;3(1):16-8.
12. Vesselle H, Schmidt RA, Pugsley JM, Li M, Kohlmyer SG, Vallières E, et al. Lung Cancer Proliferation Correlates with [F-18]Fluorodeoxyglucose Uptake by Positron Emission Tomography. Clinical Cancer Research 2000;6(10):3837-44.
13. Higashi K, Ueda Y, Yagishita M, Arisaka Y. FDG PET measurement of the proliferative potential of non-small cell lung cancer. The Journal of Nuclear Medicine 2000;41(1):85.
14. Murtaza M, Dawson S-J, Pogrebniak K, Rueda OM, Provenzano E, Grant J, et al. Multifocal clonal evolution characterized using circulating tumour DNA in a case of metastatic breast cancer. Nature Communications 2015;6:8760.
15. Newman AM, Bratman SV, To J, Wynne JF, Eclov NCW, Modlin LA, et al. An ultrasensitive method for quantitating circulating tumor DNA with broad patient coverage. Nat Med 2014;20(5):548-54.

16. Peters S, Zimmermann S. Targeted therapy in NSCLC driven by HER2 insertions. Translational Lung Cancer Research 2014;3(2):84-8.
17. Livasy CA, Karaca G, Nanda R, Tretiakova MS, Olopade OI, Moore DT, et al. Phenotypic evaluation of the basal-like subtype of invasive breast carcinoma. Mod Pathol 2005;19(2):264-71.
18. Keam B, Im S-A, Kim H-J, Oh D-Y, Kim JH, Lee S-H, et al. Prognostic impact of clinicopathologic parameters in stage II/III breast cancer treated with neoadjuvant docetaxel and doxorubicin chemotherapy: paradoxical features of the triple negative breast cancer. BMC Cancer 2007;7:203-.
19. Rhee J, Han SW, Oh DY, Kim JH, Im SA, Han W, et al. The clinicopathologic characteristics and prognostic significance of triple-negativity in node-negative breast cancer. BMC Cancer 2008;8:307.
20. Team TNLSTR. Reduced Lung-Cancer Mortality with Low-Dose Computed Tomographic Screening. New England Journal of Medicine 2011;365(5):395-409.
21. Newman AM, Lovejoy AF, Klass DM, Kurtz DM, Chabon JJ, Scherer F, et al. Integrated digital error suppression for improved detection of circulating tumor DNA. Nat Biotech 2016;34(5):547-55.
22. Pignon JP, Tribodet H, Scagliotti GV, Douillard JY, Shepherd FA, Stephens RJ, et al. Lung adjuvant cisplatin evaluation: a pooled analysis by the LACE Collaborative Group. J Clin Oncol 2008;26(21):3552-9.

Supplementary information is available in the online version of the paper

Acknowledgements We dedicate this manuscript to the memory of Roberto Macina. We also thank Samantha Navarro and Antony Tin for facilitating the PEACE ctDNA analysis presented in this manuscript. We thank the members of the TRACERx and PEACE consortia (see Supplementary Appendix for a list of centres and investigators) for participating in this study. C.S. is Royal Society Napier Research Professor. This work was supported by the Francis Crick Institute which receives its core funding from Cancer Research UK (FC001169), the UK Medical Research Council (FC001169), and the Wellcome Trust (FC001169); by the UK Medical Research Council (grant reference MR/FC001169 /1); CS is funded by Cancer Research UK (TRACERx and CRUK Cancer Immunotherapy Catalyst Network), the CRUK Lung Cancer Centre of Excellence, Stand Up 2 Cancer (SU2C), the Rosetrees Trust, NovoNordisk Foundation (ID 16584), the Prostate Cancer Foundation, the Breast Cancer Research Foundation, the European Research Council (THESEUS) and Support was provided

to CS by the National Institute for Health Research, the University College London Hospitals Biomedical Research Centre, and the Cancer Research UK University College London Experimental Cancer Medicine Centre.

Authorship contribution statement

C.A., N.J.B., G.A.W., M.J-H., T.C., R.S., and J.L-Q. contributed equally to this work. C.A. and C.S. co-wrote the manuscript. C.A., M.J.H., and C.S. conceived study design. C.A., N.J.B., G.A.W. and R.R. integrated clinicopathological data, exome data and multiplex-PCR NGS data. B.G.Z, J.L., T.C., R.S., E.K., N.S., D.H., A.N. and A.P., conducted and analysed multiplex-PCR NGS experimental work. N.J.B, G.A.W, T.B.K.W, R.R., and N.M. conducted bioinformatic analyses of TRACERx data. J.L-Q and D.A.M. conducted a central pathological review. T.M. analyzed tissue micro-array data. F.F., R.E. and F.Z. conducted central radiological review of pre-operative PET scans. H.J.W.L.A., W.L.B., F.M.F. and N.J.B. conducted volumetric analyses of pre-operative CT scans. S.V., D.J., J.L., S.S., J.C-K., A.R., T.C., D.O. and A.A. conducted technical work for TRACERx sample processing. G.E., S.W., N.M. and G.A.W. conducted TRACERx sample exome sequencing. L.M. and J.R. conducted cross-platform validation on TRACERx cell-free DNA samples. M.J.H., C.S. and M.Fa. designed the PEACE protocol. M.J.H., C.D., J.S. and C.S. designed the TRACERx protocol. C.H., S.L.M., M.F., T.A., M.Fa., E.B., D.L., M.H., S.K., N.P., S.M.J., R.T., A.A., F.B., Y.S., R.S., L.J., A.M.Q, P.C., B.N., G.M., G.L., S.T., M.N., H.R., K.K., M.C., L.G., D.F., A.N., S.R., G.A., S.K., P.R., V.E., B.I., M.I-S., V.P., J.L., M.K., R.A., H.A., H.D., S.L. are integral clinical members of TRACERx study sites. J.H. and H.L. run the UCL GCLP facility. A.H., H.B., N.I. and Y.N. were involved in study oversight. J.A.S., J.L-Q., Z.S., E.G., S.K., S.T., M.A.B, R.F.S., J.H., A.S., S.Q., P.V.L., C.D. and J.L. gave advice and reviewed the manuscript. A.H. gave statistical advice. C.S. provided overall study oversight.

Author information

The authors declare competing financial interests. Reprints and permissions information is available at www.nature.com/reprints. Correspondence should be addressed to C.S. (Charles.Swanton@crick.ac.uk).

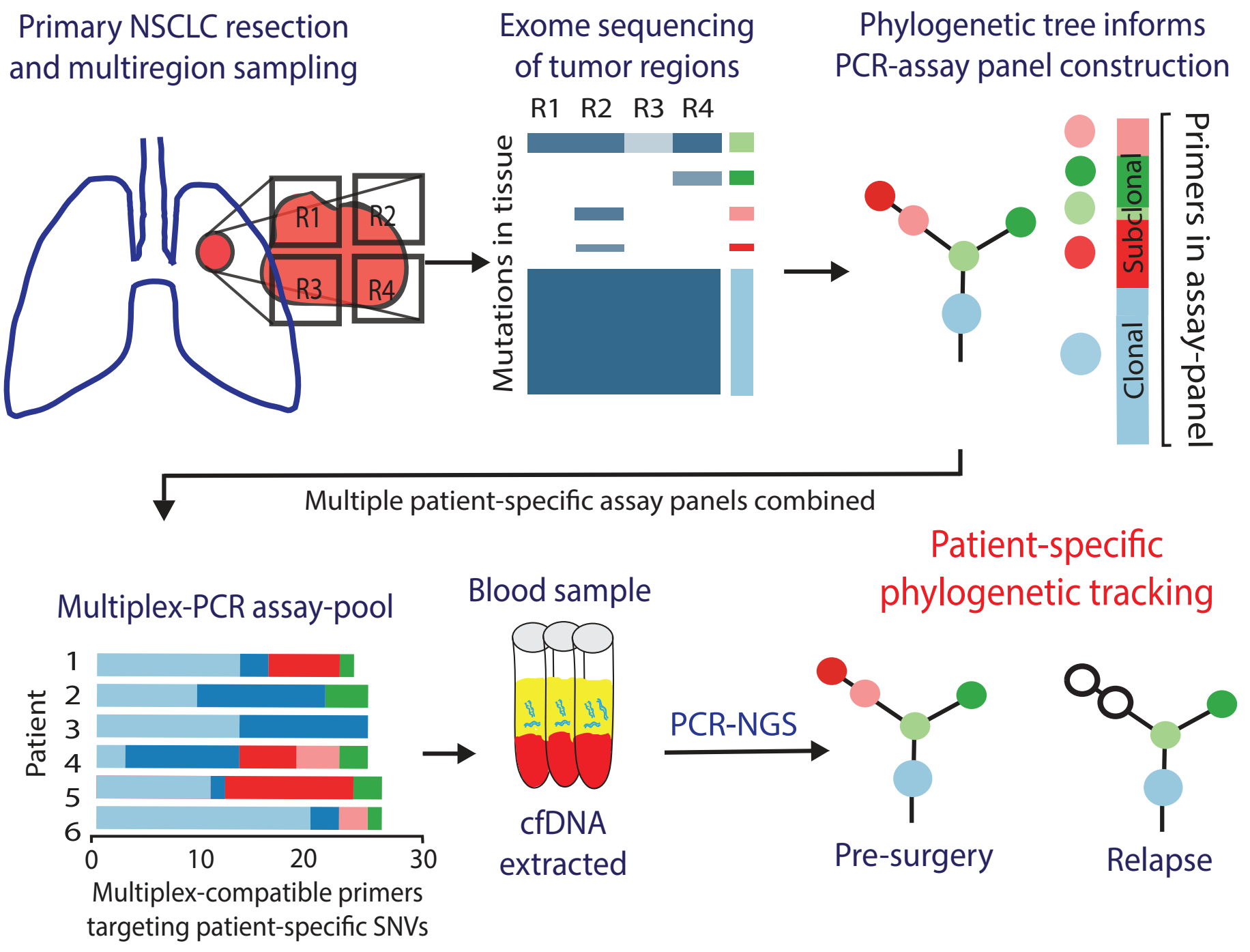
Primary NSCLC resection
and multiregion sampling
R1
R2
R3
R4
Exome sequencing
of tumor regions
R1 R2 R3 R4
Mutations in tissue
Phylogenetic tree informs
PCR-assay panel construction
Subclonal
Clonal
Primers in assay-panel
Multiple patient-specific assay panels combined
Patient-specific
phylogenetic tracking
Multiplex-PCR assay-pool
Patient
1
2
3
4
5
6
0
10
20
30
Multiplex-compatible primers
targeting patient-specific SNVs
Blood sample
cfDNA
extracted
PCR-NGS
Pre-surgery
Relapse

Figure 1 Phylogenetic ctDNA tracking

Overview of the study methodology. Multi-region sequencing of Stage I-IIIB non-small cell lung cancers was performed through the TRACERx study. Phylogenetic trees were constructed. PCR assay-panels were designed targeting clonal and subclonal single nucleotide variants to facilitate non-invasive tracking of the patient-specific tumor phylogeny. Based on predicted and validated primer compatibility assay-panels were combined into multiplex assay-pools containing primers from up to 10 patients. Cell-free DNA was extracted from pre and post-operative plasma samples and multiplex-PCR performed. This was followed by next generation sequencing of amplicons. Findings were integrated with M-Seq exome data to track tumor evolution.

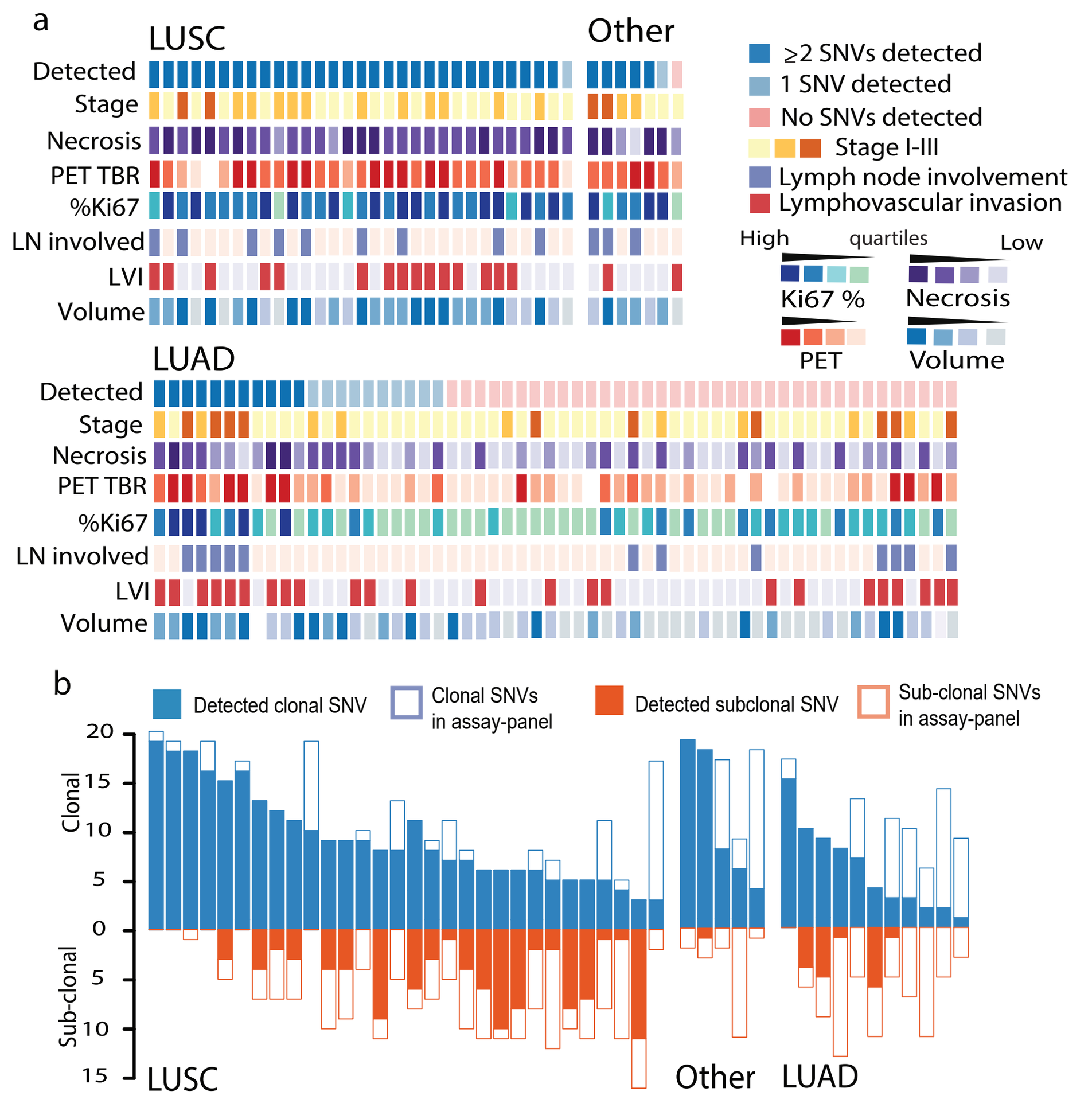
a
LUSC
Other
Detected
Stage
Necrosis
PET TBR
%Ki67
LN involved
LVI
Volume
≥2 SNVs detected
1 SNV detected
No SNVs detected
Stage I-III
Lymph node involvement
Lymphovascular invasion
High
quartiles
Low
Ki67 %
Necrosis
PET
Volume
LUAD
Detected
Stage
Necrosis
PET TBR
%Ki67
LN involved
LVI
Volume
b
Detected clonal SNV
Clonal SNVs in assay-panel
Detected subclonal SNV
Sub-clonal SNVs in assay-panel
Clonal
Sub-clonal
20
15
10
5
0
5
10
15
LUSC
Other
LUAD

Figure 2 – Clinicopathological predictors of ctDNA detection

a) Heatmap showing clinicopathological and ctDNA detection data, continuous variables quartiled. Raw data and patient IDs in Supplementary Table 1. b) Detection of clonal and subclonal single nucleotide variants within 46 patients with two or more single nucleotide variants detected in plasma. Histology indicated in panels as LUSC, LUAD and Other. Other histology refers to large cell carcinoma (1/1 ctDNA positive), adenosquamous carcinoma (2/3 ctDNA positive), large cell neuroendocrine carcinoma (1/1 ctDNA positive) and carcinosarcoma (1/2 ctDNA positive).

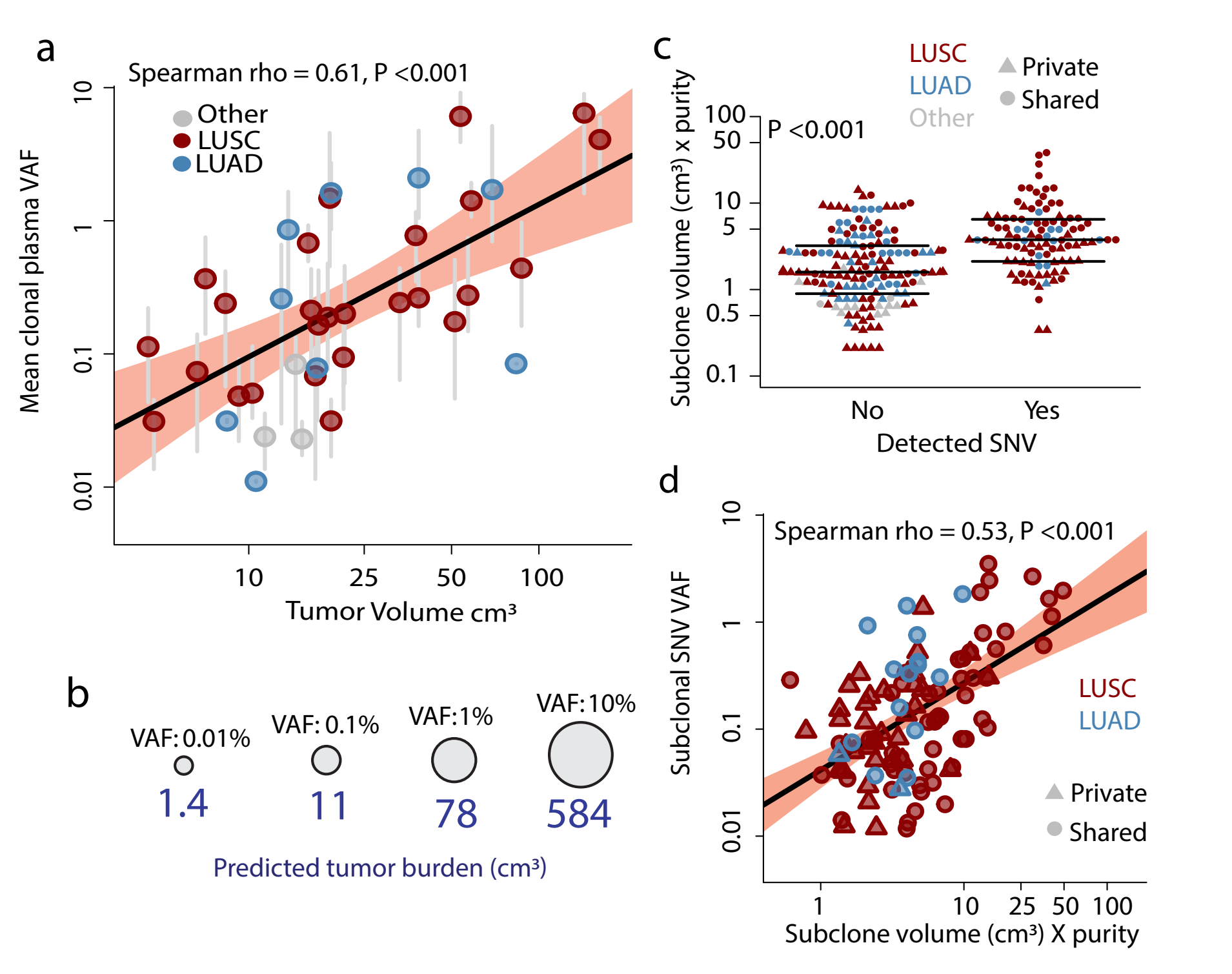
a
Spearman rho = 0.61, P <0.001
Other
LUSC
LUAD
Mean clonal plasma VAF
10
1
0.1
0.01
10
25
50
100
Tumor Volume cm³
b
VAF: 0.01%
VAF: 0.1%
VAF:1%
VAF:10%
1.4
11
78
584
Predicted tumor burden (cm³)
c
LUSC
LUAD
Other
Private
Shared
P <0.001
Subclone volume (cm³) x purity
100
50
10
5
1
0.5
0.1
No
Yes
Detected SNV
d
Spearman rho = 0.53, P <0.001
Subclonal SNV VAF
10
1
0.1
0.01
1
10
25
50
100
Subclone volume (cm³) X purity
LUSC
LUAD
Private
Shared

Figure 3. Tumor volume predicts plasma variant allele frequency

a) Tumor volume (cm^3) measured by CT volumetric analysis correlates with mean clonal plasma VAF, n=38, grey vertical lines represent range of clonal VAF, line of best fit estimated in log-space, 95% confidence intervals indicated by red shading. b) Predicted tumor burden at hypothetical clonal VAF intervals ranging from 0.01% to 10% based on linear model shown in panel a. c) Estimated effective subclone size, defined as mean CCF of subclone across sampled tumor regions multiplied by effective tumor volume (volume × purity), influences subclonal SNV detection. For negative calls, median effective subclone size was 1.60 cm^3, range= 0.21-14.11, n=163 for positive calls, median effective subclone size = 3.97 cm^3, range = 0.33 – 45.09, n=109. Wilcoxon rank sum test, $P<0.001$, data from 34 patients (who passed volumetric filters and had subclonal SNVs represented in assay-panel). d) Estimated effective subclone size correlates with subclonal plasma VAF, n=109 subclonal SNVs, data from 24 patients (who passed volumetric filters with detected subclonal SNVs in plasma).

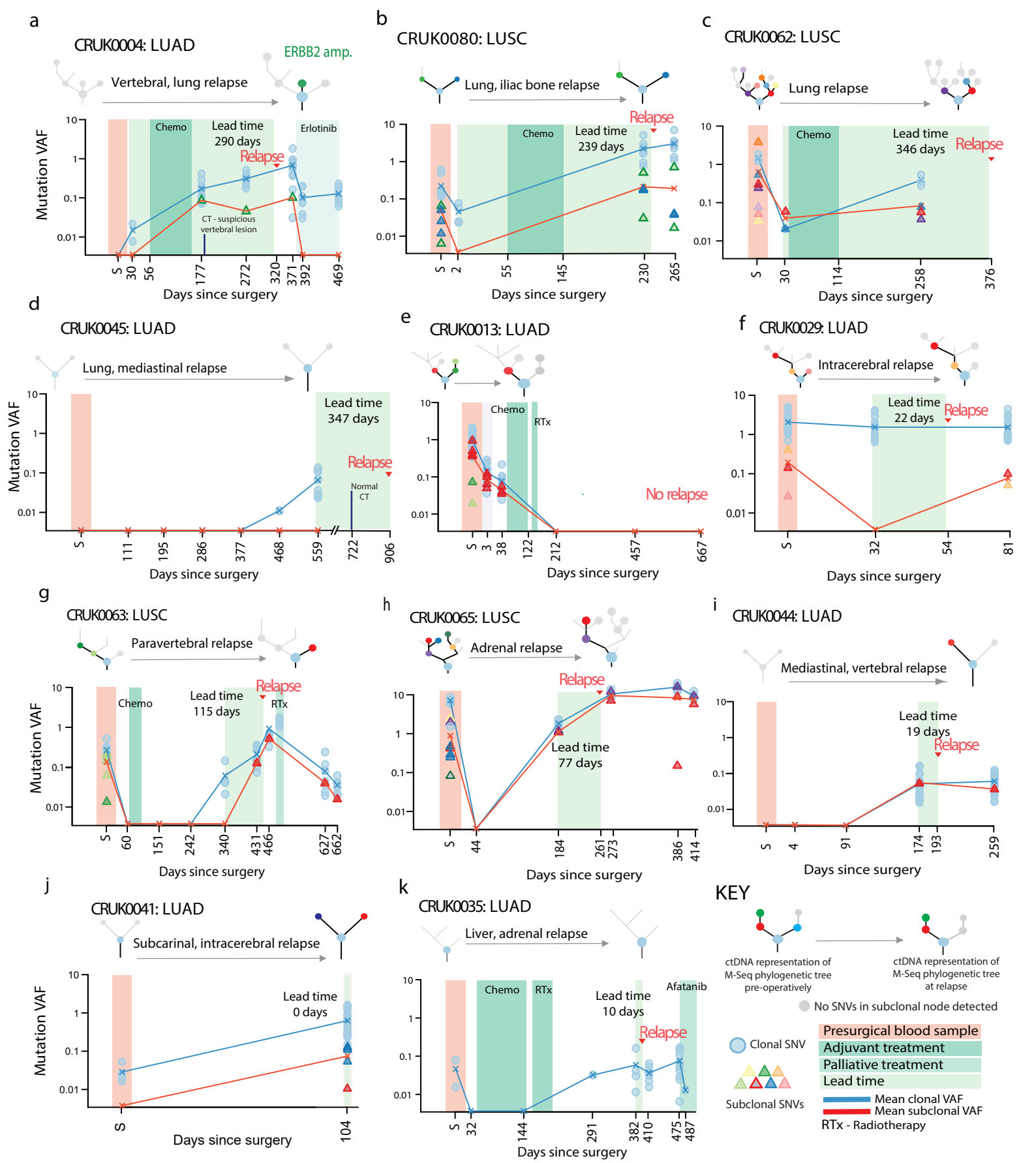
a
CRUK0004: LUAD
ERBB2 amp.
Vertebral, lung relapse
Chemo
Lead time
290 days
Erlotinib
Relapse
CT - suspicious
vertebral lesion
Mutation VAF
Days since surgery
b
CRUK0080: LUSC
Lung, iliac bone relapse
Relapse
Chemo
Lead time
239 days
Days since surgery
c
CRUK0062: LUSC
Lung relapse
Chemo
Lead time
346 days
Relapse
Days since surgery
d
CRUK0045: LUAD
Lung, mediastinal relapse
Lead time
347 days
Relapse
Normal
CT
Mutation VAF
Days since surgery
e
CRUK0013: LUAD
Chemo
RTx
No relapse
Days since surgery
f
CRUK0029: LUAD
Intracerebral relapse
Lead time
22 days
Relapse
Days since surgery
g
CRUK0063: LUSC
Paravertebral relapse
Chemo
Lead time
115 days
Relapse
RTx
Mutation VAF
Days since surgery
h
CRUK0065: LUSC
Adrenal relapse
Relapse
Lead time
77 days
Days since surgery
i
CRUK0044: LUAD
Mediastinal, vertebral relapse
Lead time
19 days
Relapse
Days since surgery
j
CRUK0041: LUAD
Subcarinal, intracerebral relapse
Lead time
0 days
Mutation VAF
Days since surgery
k
CRUK0035: LUAD
Liver, adrenal relapse
Chemo
RTx
Lead time
10 days
Afatanib
Relapse
Days since surgery
KEY
ctDNA representation of
M-Seq phylogenetic tree
pre-operatively
ctDNA representation of
M-Seq phylogenetic tree
at relapse
No SNVs in subclonal node detected
Clonal SNV
Subclonal SNVs
Presurgical blood sample
Adjuvant treatment
Palliative treatment
Lead time
Mean clonal VAF
Mean subclonal VAF
RTx - Radiotherapy

Figure 4 – Post-operative ctDNA detection predicts and characterizes NSCLC relapse – 2a-k) Longitudinal cell-free DNA profiling. Circulating tumor DNA (ctDNA) detection in plasma was defined as the detection of two tumor-specific SNVs. Relapse was based on imaging-confirmed NSCLC relapse, imaging was performed as clinically indicated. Detected clonal (circles, light blue) and subclonal (triangles, colors indicates different subclones) SNVs from each patient-specific assay-panel are plotted on graphs colored by M-Seq derived tumor phylogenetic nodes. Mean clonal (blue) and mean subclonal (red) plasma VAF are indicated on graphs as connected lines. Pre-operative and relapse M-Seq derived phylogenetic trees represented by ctDNA are illustrated above each graph.

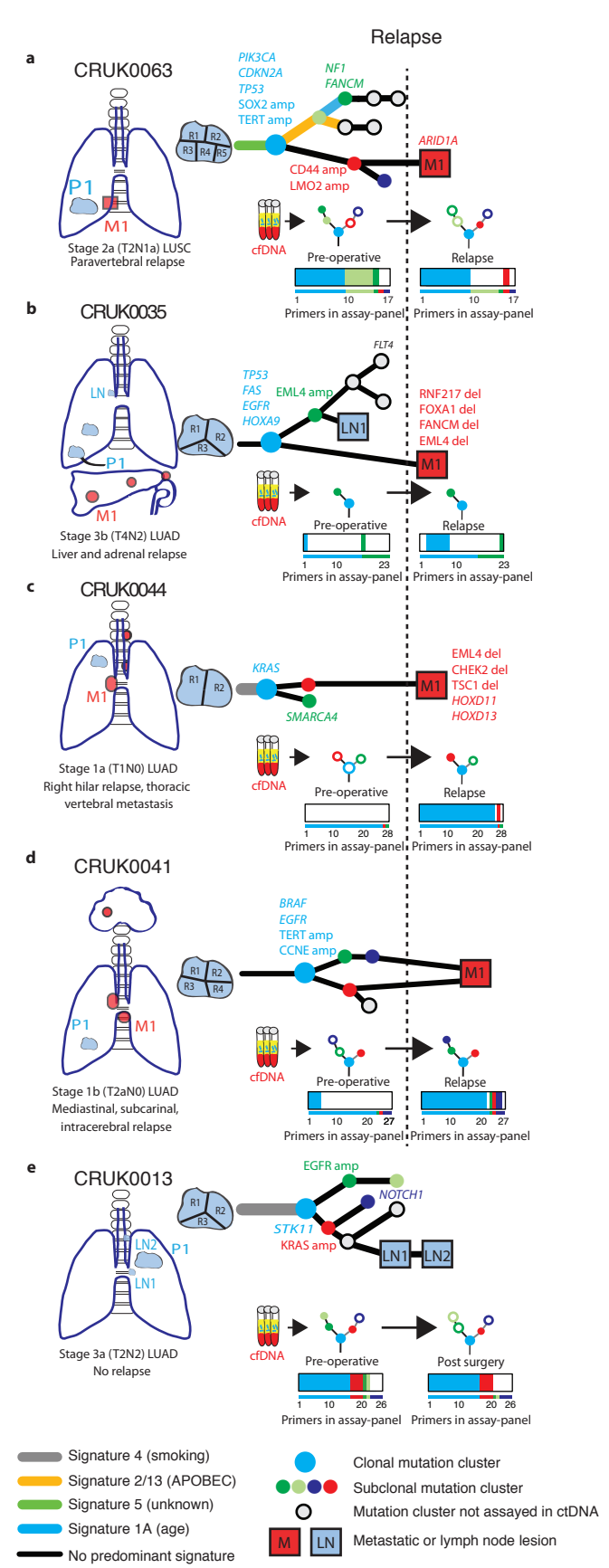
Relapse
a
CRUK0063
P1
M1
Stage 2a (T2N1a) LUSC
Paravertebral relapse
PIK3CA
CDKN2A
TP53
SOX2 amp
TERT amp
NF1
FANCM
ARID1A
M1
CD44 amp
LMO2 amp
R1
R2
R3
R4
R5
cfDNA
Pre-operative
Relapse
1 10 17
Primers in assay-panel
b
CRUK0035
LN
P1
M1
Stage 3b (T4N2) LUAD
Liver and adrenal relapse
FLT4
TP53
FAS
EGFR
HOXA9
EML4 amp
LN1
RNF217 del
FOXA1 del
FANCM del
EML4 del
M1
1 10 23
c
CRUK0044
P1
M1
Stage 1a (T1N0) LUAD
Right hilar relapse, thoracic
vertebral metastasis
KRAS
SMARCA4
EML4 del
CHEK2 del
TSC1 del
HOXD11
HOXD13
M1
1 10 20 28
d
CRUK0041
P1
M1
Stage 1b (T2aN0) LUAD
Mediastinal, subcarinal,
intracerebral relapse
BRAF
EGFR
TERT amp
CCNE amp
M1
1 10 20 27
e
CRUK0013
LN2
P1
LN1
Stage 3a (T2N2) LUAD
No relapse
EGFR amp
NOTCH1
STK11
KRAS amp
LN1
LN2
Post surgery
1 10 20 26
Signature 4 (smoking)
Signature 2/13 (APOBEC)
Signature 5 (unknown)
Signature 1A (age)
No predominant signature
Clonal mutation cluster
Subclonal mutation cluster
Mutation cluster not assayed in ctDNA
M
LN
Metastatic or lymph node lesion

Figure 5. **Re-design of phylogenetic trees to incorporate relapse tissue sequencing data to benchmark post-operative ctDNA analyses**

Phylogenetic trees based on mutations found in primary and metastatic tissue (a-d), or primary tumor and lymph node biopsies (e). Colored nodes in phylogenetic trees indicate cancer clones harboring mutations assayed for in ctDNA, grey indicates a clone not assayed. Thick colored bar shows number of assays per sample detected preoperatively and at relapse (a-d) or in the absence of relapse, post surgery (e). Thin colored bar shows number of assays in total. Colors matches clones on the phylogenetic trees.

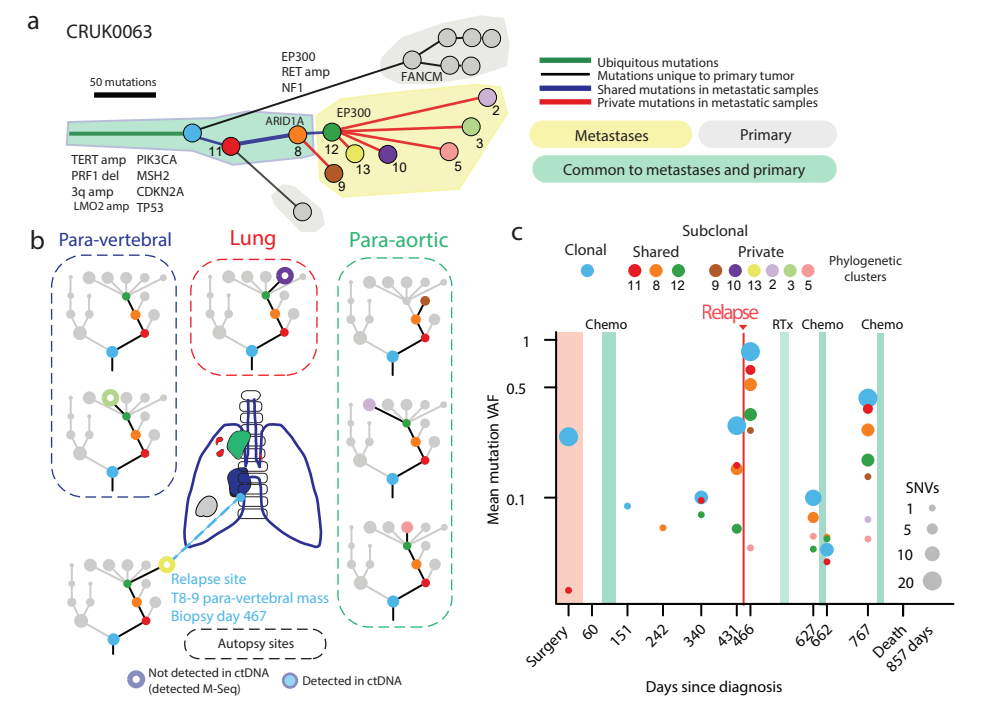
a
CRUK0063
50 mutations
EP300
RET amp
NF1
FANCM
ARID1A
EP300
TERT amp
PRF1 del
3q amp
LMO2 amp
PIK3CA
MSH2
CDKN2A
TP53
Ubiquitous mutations
Mutations unique to primary tumor
Shared mutations in metastatic samples
Private mutations in metastatic samples
Metastases
Primary
Common to metastases and primary
b
Para-vertebral
Lung
Para-aortic
Relapse site
T8-9 para-vertebral mass
Biopsy day 467
Autopsy sites
Not detected in ctDNA
(detected M-Seq)
Detected in ctDNA
c
Subclonal
Clonal
Shared
Private
Phylogenetic clusters
Chemo
Relapse
RTx
Chemo
Chemo
Mean mutation VAF
SNVs
Surgery
Death
Days since diagnosis

Figure 6. ctDNA tracking of lethal cancer subclones in CRUK0063

Sampling and sequencing was performed of one relapse biopsy at day 467 and five metastatic tissue samples from three lesions at time of death through the PEACE (Posthumous Evaluation of Advanced Cancer Environment) post mortem study. Phylogenetic analysis revealed cancer evolution and identified private subclones at each site. **a).** To-scale phylogenetic tree of CRUK0063 including M-seq based on metastatic and primary tumor regions. Branch length is proportional to number of mutations in each subclone. Colors represents mutation clusters, light blue node representing the clonal cluster. **b)** Tissue-specific phylogenetic trees for metastatic lesions, highlighted nodes in color represents mutation clusters found at each site and assayed for in ctDNA. Open circles represents mutation clusters not detected at any time in ctDNA. **c)** Tracking plot of identified subclones in ctDNA, showing mean VAF of identified subclones. Size of dots indicates number of assays detected. Colors corresponds to mutation clusters and matches panels a and b. Tiered burden of subclonal disease can be observed, with clusters representing earlier cancer subclones present at higher VAF, likely reflecting a larger cancer burden carrying shared relative to private mutations.